Influence of Aspect Ratio and Wettability on Residual Oil Saturations after Waterflooding and Immiscible Gas Flooding: A Microfluidics Based Study

Sushobhan Pradhan[1], Gbeu Kone[1], Ryan Antle[2], Clint Aichele[1], Haifeng Jiang[2,*] and Prem Bikkina[1,*]
[1] Oklahoma State University, Stillwater, Oklahoma, USA
[2] Oil & Gas Technology Center, Baker Hughes, a GE Company, Oklahoma City, Oklahoma, USA
*Corresponding Author

This paper was prepared for presentation at the International Symposium of the Society of Core Analysts held in Trondheim, Norway, 27-30 August 2018

ABSTRACT

A series of microfluidic experiments have been carried out to understand the influence of aspect ratio (AR) and wettability on residual oil saturations (S_{or}) in water and immiscible gas flooding. Linear and uniform pore network microfluidic chips with various wettability, ARs and depths were used. Water, n-decane, and methane were used as aqueous, oil, and gas phases, respectively. Water and oil were dyed with 1 g/l concentrations of methyl blue and Sudan red, respectively, for better visual contrast for the fluid saturation measurements. 0.1 µL/min flow rate was used during oil saturation and water flooding and 0.3 sccm flow rate was used for gas flooding to maintain the capillary numbers in the range of 10^{-7} to 10^{-5} to be in compliance with typical reservoir capillary numbers. An image analysis protocol using ImageJ was used to measure the residual fluid saturations.

Linear pore networks of 20 µm and 40 µm depths with same ARs were used to study the influence of depth on residual fluid saturations. It has been found that the depth has a significant influence on the pore-scale residual fluid saturations. For 20 µm depth chips, pore-scale residual oil saturation after waterflooding (S_{orw}) increased with the AR semi-logarithmically (log AR vs. S_{orw}) for both hydrophilic and hydrophobic chips. The pore-scale S_{orw} for 40 µm depth hydrophobic chips also followed the same trend, however, the 40 µm depth hydrophilic chips exhibited an exponential trend.

Uniform pore networks with same depth were also used to study the effect of AR on residual saturations. For hydrophilic uniform pore networks, the chip-scale S_{orw} data spread between 41 and 51 %PV for the AR range of 1.97 to 23.94, the data for hydrophobic uniform pore networks fall between 72 and 57 %PV, respectively. For both the hydrophilic and hydrophobic uniform pore networks, there exits strong semi-logarithmic relationships between AR and residual oil saturation after gas flooding (log AR vs. S_{org}). The data can be used to validate flow simulation models in digital rock analysis.

Keywords: aspect ratio, wettability, residual oil saturation, waterflooding, gas flooding, pore-scale, chip-scale, ImageJ

INTRODUCTION

Crude oil is typically produced in primary, secondary, and tertiary recovery stages. Waterflooding and gas flooding are widely used secondary and tertiary oil recovery techniques. Oil recovery performances of waterflooding and gas flooding are known to be varied significantly. For example, a wide range (less than 10% to up to 80 %OOIP) of oil recovery efficiencies have been reported for waterflooding [1]. Variation in rock and fluid properties could have caused for this huge range in the oil recovery [1]. The recovery efficiencies are known to be controlled by both microscopic (pore-scale) and macroscopic (core-/reservoir-scale) sweeping efficiencies. While phenomena such as gravity override, thief zones, and viscous fingering are responsible for reduced core-/reservoir-scale sweeping efficiencies, wettability and pore-throat aspect ratio influence the pore-scale displacement efficiency. There have been numerous experimental and modeling studies on the influence of wettability on waterflooding and gas flooding efficiencies at core- and reservoir scales [2-4]. But, there are very limited number of studies on the influence of wettability and aspect ratio on pore-scale sweeping efficiency [5]. Hence, this work attempts to investigate the effect of pore-scale and chip-scale sweeping efficiencies of waterflooding and gas flooding in hydrophilic and hydrophobic porous media with a wide range of aspect ratios. In recent years, microfluidics has been gaining acceptance for petroleum engineering research especially for understanding oil trapping and recovery mechanisms in the porous media [6-8]. The major advantages of using microfluidics for these studies include flexibility in porous media chip design in a highly controlled and reproducible manner, easy and accurate control of fluid flow, and most importantly the ability to visually study the involved oil recovery mechanisms both at pore- and chip-scales. In this study, systematic microfluidic experiments have been conducted to quantify the influence of pore-scale and chip-scale performances of waterflooding and gas flooding. Hydrophobic and hydrophilic linear and uniform pore network microfluidic chips of aspect ratios ranging from 1.97 to 60.16 were designed and used for waterflooding experiments followed by gas flooding experiments with a state-of-the-art microfluidics facility. The residual fluid saturations were measured using ImageJ.

MATERIALS AND METHODS

Materials

Water, n-Decane, and CH_4 were used as aqueous, oil, and gas phases, respectively. The aqueous and oil phases were dyed with methyl blue and Sudan red to increase visual contrast for enhanced fluid saturation measurements. Further details of the fluids used are given in Table 1.

Table 1. Fluids used in microfluidic experiments

Water phase	DI water, dyed with Methyl blue at 1g/L
Oil phase	n-decane 99% purity, dyed with Sudan red at 1g/L
Gas phase	CH_4, ultra-high purity grade

Chip Design

To study the influence of AR and wettability on pore scale and chip scale waterflooding and gas flooding behavior, eight different types of linear pore networks and four different types of uniform porous media networks were designed and procured. In this study, AR was defined as the ratio of maximum cross-sectional areas of the pore and the throat, both measured perpendicular to the flow direction.

Figure 1(a) shows the four uniform pore network designs with different ARs, achieved by varying the pore width while keeping all the other parameters same. The ARs of the designs are 1.97, 5.83, 11.87, and 23.94.

Figure 1(b) and 1(c) show the designs 5 and 6, both are linear pore networks. Design 5 has five individual linear pores of different ARs (1.97, 5.83, 11.87, 23.94, and 60.16). Design 6 contains three individual linear pores with ARs of 5.83, 11.87, and 23.94, but with 40 µm depth of pores and throats comparing the regular depth of 20 µm. Each design was made into both hydrophilic and hydrophobic chips with the same dimensions.

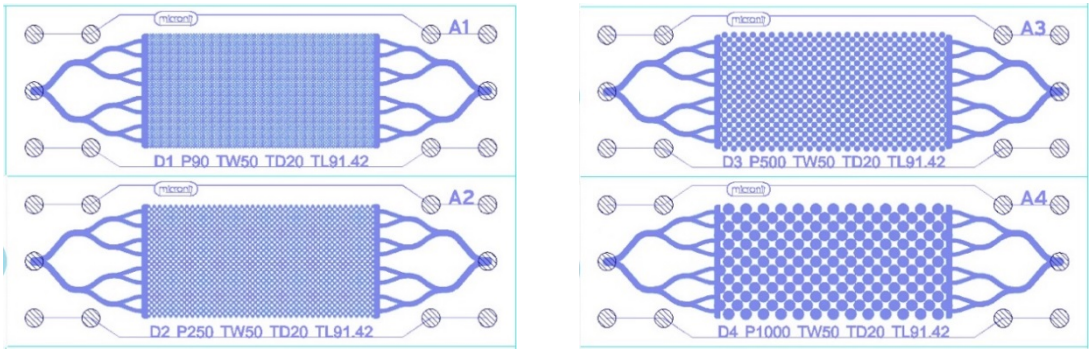

Figure 1 (a): Uniform pore network chip designs 1 to 4

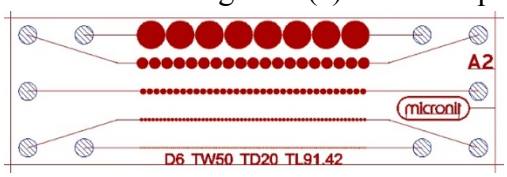

Figure 1 (b): Design 5 linear pore network

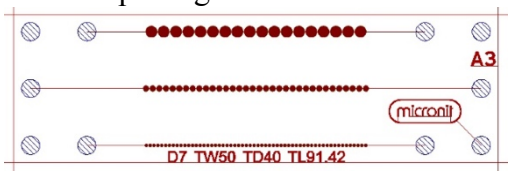

Figure 1 (c): Design 6 linear pore network

Notation: D: Design; P: Pore width; TW: Throat Width; TD: Throat Depth; TL: Throat Length

Experimental Facility

The schematic of the microfluidics setup used in this study is shown in Figure 2. It consists of three microfluidic pumps for fluid injections, operated by a compressed air source of 125 psig. The pumps are connected to a 6-position selector valve at inlet 1, 2, and 3. Gas (Methane) injection is handled by an ultra-low gas mass flow controller connected to inlet 4 on the 6-position selector valve. The outlet from the selector valve is connected to the microfluidics chip via a manual 3-way valve (Valve #1), which can also bypass the chip through a bypass line. The pressure is held by an ultra-high sensitivity back pressure regulator (BPR) set at 100 psig supplied by a helium gas cylinder.

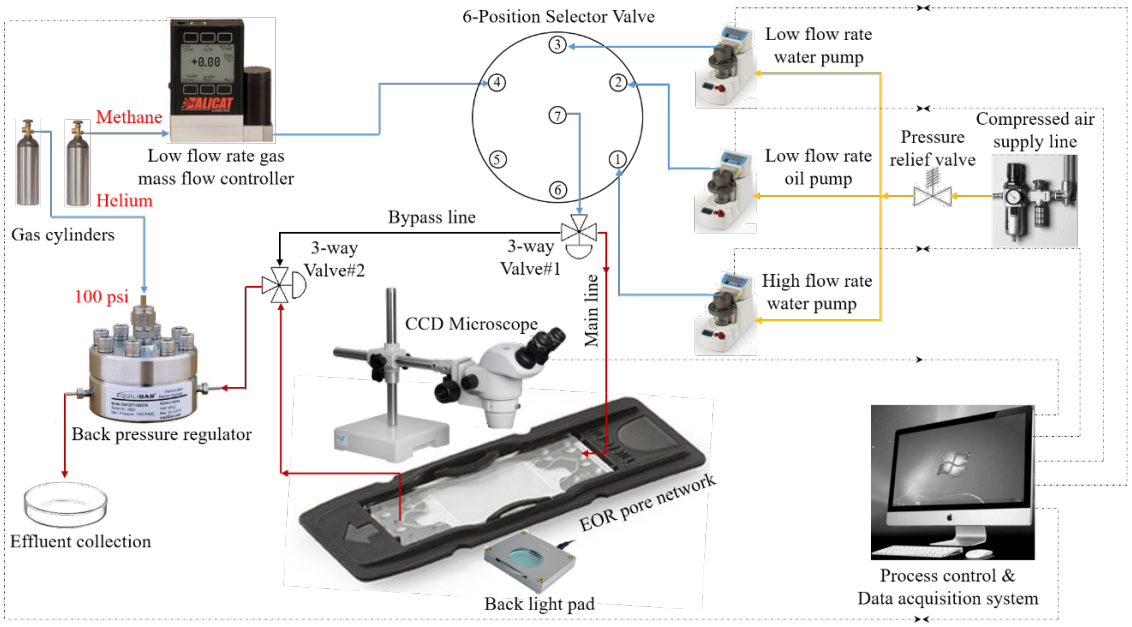

Figure 2: Microfluidics experimental facility

Experimental Procedures

In each experiment, a microfluidic chip was first saturated with water then oil to achieve the initial saturations (S_{wi} and S_{oi}). It was then flooded with water followed by gas to achieve residual fluid saturations (S_{orw} and S_{org}). Water and gas injection rates were adjusted to be 0.1 µl/min and 0.3 sccm, respectively, to maintain capillary numbers in the range of 10^{-7} to 10^{-5}, to match values of reservoirs. A constant back pressure of 100 psig was maintained throughout the experiment. Chip and pore scale images were taken, and analyzed using ImageJ software to measure the residual fluid saturations.

RESULTS AND DISCUSSION

Linear Pore Network

Effect of AR on S_{oi}, S_{orw}, and S_{org} in Hydrophilic and Hydrophobic Linear Networks

1. Effect of AR on S_{oi}

20 µm depth hydrophilic and hydrophobic linear pore networks of ARs ranging from 1.97 to 60.16 were used in this set of experiments. As can be seen in Figure 3, in all the hydrophilic chips, 100% of the bulk water was displaced by oil regardless of the AR after the oil saturation; whereas in the case of hydrophobic chips, as the AR increases from 1.97 to 60.16, the S_{oi} decreases from 100 %PV to 77.7 %PV. The two insets in Figure 3 show two pores each of AR 60.16 hydrophilic and hydrophobic linear pore networks at S_{oi}.

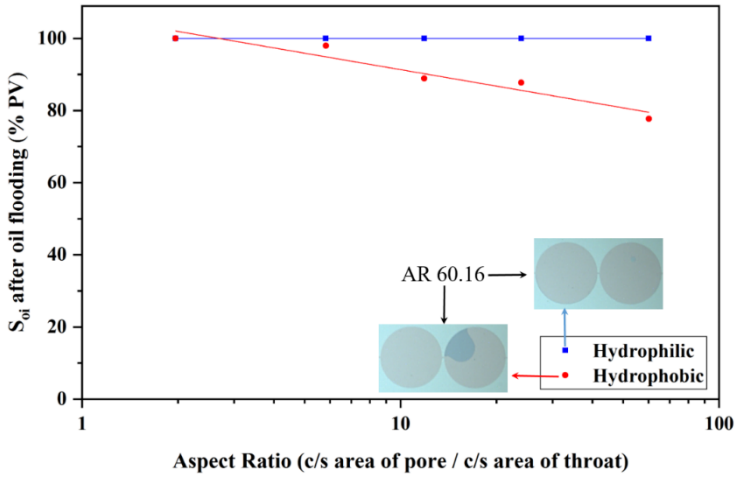

Figure 3: S_{oi} in 20 µm depth hydrophilic and hydrophobic linear pore networks

2. Effect of AR on S_{orw}

The chips from previous step (at S_{oi}) were waterflooded to reach irreducible oil saturations (S_{orw}). As can be seen in Figure 4(a) and 4(b), similar semi-logarithmic relationships exist between S_{orw} and AR in both hydrophilic and hydrophobic linear networks. Capillary number (N_{ca}) was calculated using the equation below:

$$N_{ca} = \frac{\mu v}{\sigma \cos\theta}$$

Where: μ is the viscosity of water phase, v is the fluid velocity in-situ, σ is the interfacial tension (IFT) between water and oil phase, and θ is the contact angle.

Based on the three-phase contact lines observed in the pores, contact angles of 20° and 100° were used for hydrophilic and hydrophobic networks. The n-decane/water IFT was 52 mN/m. Inferring from the trends of AR vs. S_{orw} and N_{ca} vs. S_{orw}, under the same injection rate, the observed increase in the S_{orw} with higher ARs may be due to the decrease in the displacing fluid velocity in the larger pores.

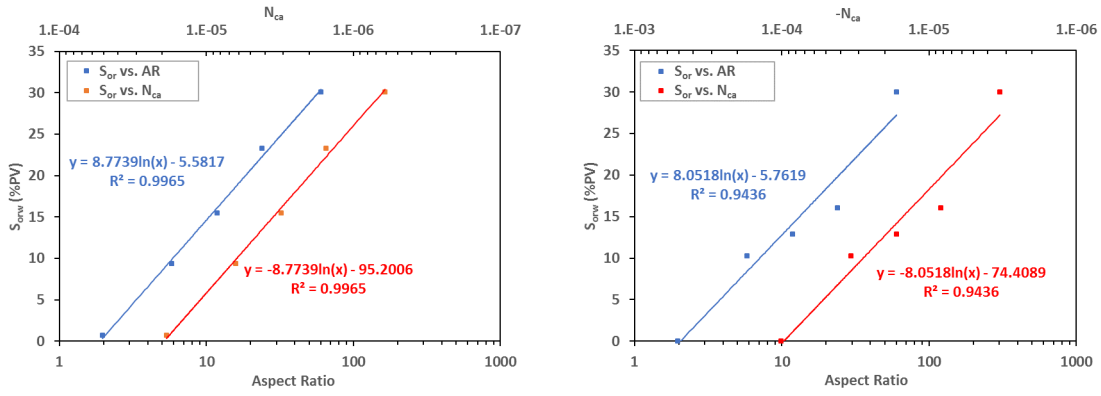

(a) Hydrophilic (b) Hydrophobic

Figure 4: Effect of AR and N_{ca} vs. S_{orw} in 20 µm depth linear pore networks

3. Effect of AR on S_{org}

The previously waterflooded chips (at S_{orw}) were then gas flooded to reach irreducible oil saturations (S_{org}). As can be seen in Figure 5, hydrophilic and hydrophobic chips exhibited similar trends and S_{org} values at higher ARs (23.94 and 60.16); however, at low ARs (1.97, 5.83, and 11.87), hydrophilic chips achieved significantly lower S_{org} compared to hydrophobic chips.

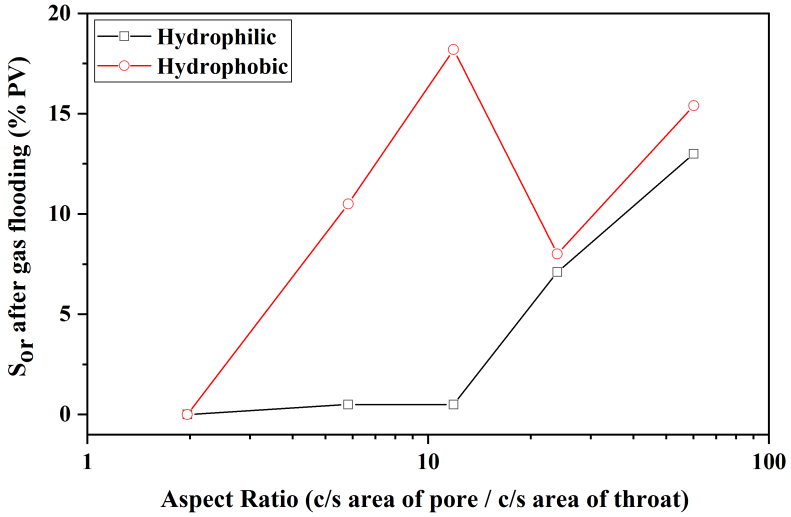

Figure 5: Effect of AR on S_{org} in hydrophilic and hydrophobic linear pore networks

In hydrophilic networks, water is the most wetting fluid, so gas as the most non-wetting phase displaces oil more effectively resulting in lower residual oil saturation; In hydrophobic networks, oil is the most wetting fluid so gas displaces water more effectively resulting in higher residual oil saturation. However, when AR's are higher (exceeding 11.87 in this study), the difference becomes negligible indicating an additional effect from AR which takes effect only at higher AR's.

Effect of channel depth on S_{oi}, S_{orw} and S_{org} in hydrophilic and hydrophobic linear pore networks

Chips with same ARs but different channel depth (40 µm) were used in this set of experiments. Table 2 shows the oil saturations at different stages of the experiments (S_{oi}, S_{orw}, S_{org}).

Table 2. S_{oi} and S_{org} (%PV) in 40 µm depth linear pore networks

	Hydrophilic Chip			Hydrophobic Chip		
Aspect Ratio	**S_{oi} (%PV)**	**S_{orw} (%PV)**	**S_{org} (%PV)**	**S_{oi} (%PV)**	**S_{orw} (%PV)**	**S_{org} (%PV)**
23.94	84.5	34.8	6	92.1	2	0.3
11.87	94.2	5.5	2	90.4	0.9	0.9
5.83	88.6	2.4	4.5	99.7	0	0

Figure 6 (a) and (b) show the comparison of oil saturations at each state between 20 µm and 40 µm depths at different ARs. For hydrophilic chips, the depth did affect the initial oil saturation. However, for hydrophobic chips, both depths showed same initial saturations, while 40 µm depth hydrophobic chips exhibited significantly lower residual oil saturations post waterflooding and gas flooding.

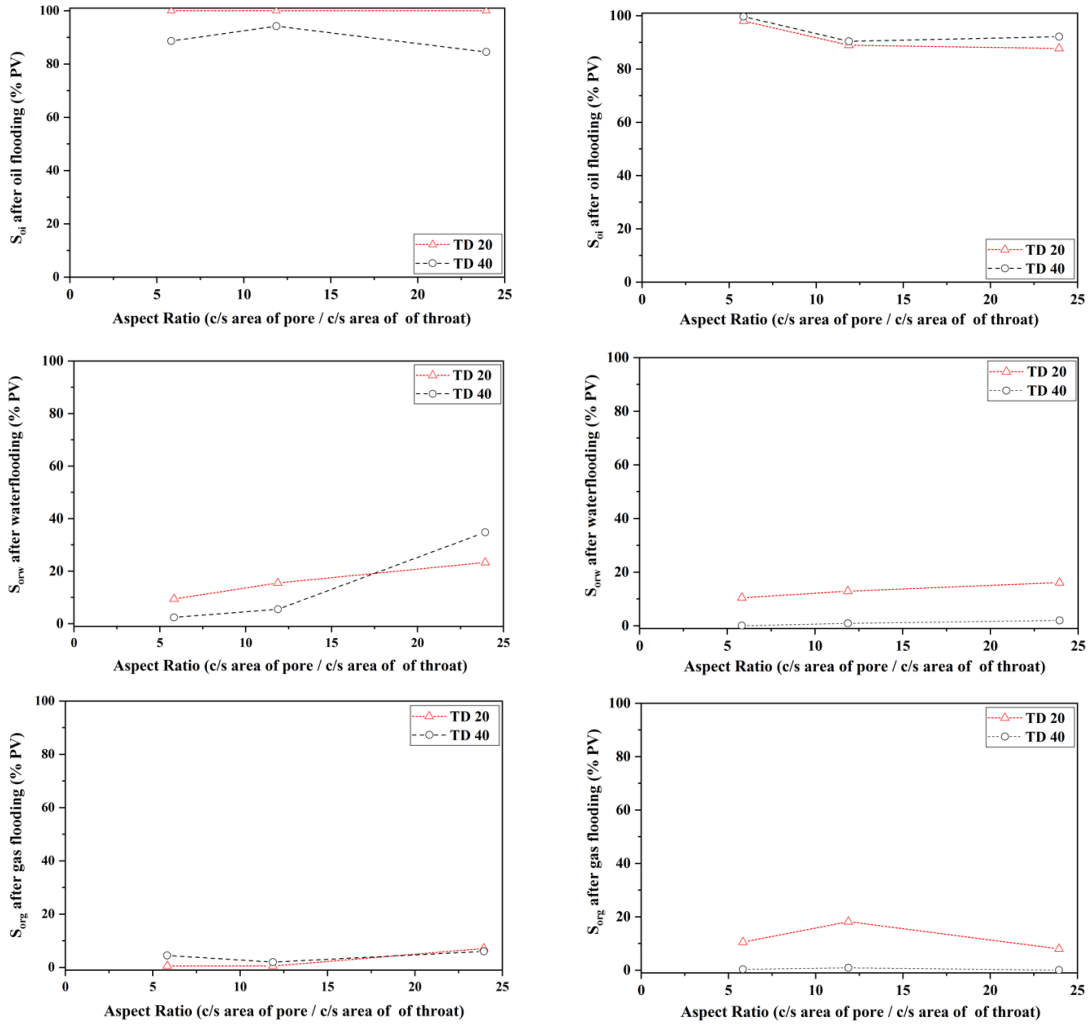

(a) Hydrophilic (b) Hydrophobic

Figure 6: AR vs. S_{oi}, S_{orw}, and S_{org} in 20 µm and 40 µm depth linear pore networks

Uniform Pore Network

Same waterflooding and gas flooding experiments were also conducted on uniform networks with different ARs and wetting conditions, and 20 µm channel depth.

Effect of AR on S_{orw}, S_{org} and S_g

As shown in Figure 7(a), no clear trend was observed between AR on S_{orw} for hydrophilic uniform pore network chips. In the linear pore networks, residual non-wetting phase saturation only occurs due to snap-off phenomenon whereas in the uniform pore networks, the trapping can also occur via other modes such as mentioned in pore doublet model and dead-end model [9].

Similar to hydrophilic uniform pore network chips, no clear trend was observed between AR on S_{orw} for hydrophobic uniform pore network chips. The S_{orw} range of the hydrophobic chips (i.e., 72 to 57 %PV) is considerably higher than the range of the hydrophilic chips (i.e., 41 to 51 %PV). Unlike in the case of waterflooding, there exist semi-logarithmic relationships (as shown in Figure 7(a) between S_{org} and AR in the case of hydrophilic and hydrophobic uniform pore networks. As shown in Figure 7(b), linear trends were observed between AR on S_g in both hydrophilic and hydrophobic uniform pore network chips.

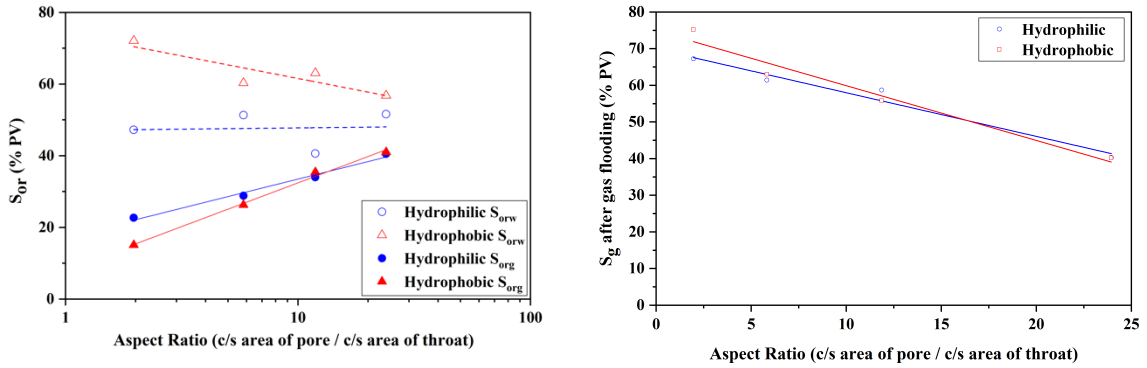

(a) AR vs. S_{org} and S_{orw} (b) AR vs. S_g

Figure 7: Effect of AR on saturations in uniform pore networks

In gas flooding, as the AR increases, S_{org} in hydrophilic and hydrophobic chips become closer which implies AR has equal or even stronger influence on S_{org} compared to the effect of wettability.

CONCLUSIONS

- Aspect ratio has significant effects on oil saturations at different stages of the experiments (S_{oi}, S_{orw}, and S_{org}) in linear pore networks. In general, higher aspect ratio results in higher residual oil saturations after water and gas flooding. Calculations of capillary numbers (N_{ca}) confirmed that the effect may be due to the reduction of injection fluid velocity in larger pores at higher aspect ratios.
- Depth has a significant influence on the pore-scale residual fluid saturations. For hydrophilic chips, the depth did affect the initial oil saturation. However, for hydrophobic chips, both depths showed same initial saturations, while 40 µm depth hydrophobic chips exhibited significantly lower residual oil saturations post waterflooding and gas flooding.

- For uniform pore networks, both hydrophilic and hydrophobic networks showed strong semi-logarithmic relationships between AR and residual oil saturation after gas flooding (log AR vs. S_{org}) and linear relationships between AR and S_g.
- For uniform pore networks, the results indicated higher gas saturation (S_g) at lower aspect ratios with smaller pore sizes; the high gas saturation contributed to increased oil recovery (lower residual oil saturation) post gas flooding.
- By comparing residual oil saturations post water and gas flooding in uniform networks, it shows that at higher aspect ratios, the difference between S_{orw} and S_{org} becomes narrower, indicting less incremental potential for immiscible gas EOR.

ACKNOWLEDGEMENTS

The authors gratefully acknowledge Baker Hughes, a GE Company (BHGE) for their technical and financial support throughout the research project.

REFERENCES

1. Wardlaw, N. and J. Cassan, *Oil recovery efficiency and the rock-pore properties of some sandstone reservoirs.* Bulletin of Canadian Petroleum Geology, 1979. **27**(2): p. 117-138.
2. Rao, D., M. Girard, and S. Sayegh, *The influence of reservoir wettability on waterflood and miscible flood performance.* Journal of Canadian Petroleum Technology, 1992. **31**(06).
3. Jadhunandan, P. and N.R. Morrow, *Effect of wettability on waterflood recovery for crude-oil/brine/rock systems.* SPE reservoir engineering, 1995. **10**(01): p. 40-46.
4. Bikkina, P., Wan, J., Kim, Y., Kneafsey, T.J. and Tokunaga, T.K., *Influence of wettability and permeability heterogeneity on miscible CO_2 flooding efficiency*. Fuel, 2016. **166**, p. 219-226.
5. Wardlaw, N., *The effects of geometry, wettability, viscosity and interfacial tension on trapping in single pore-throat pairs.* Journal of Canadian Petroleum Technology, 1982. **21**(03).
6. Sohrabi, M.T.D.H., Tehrani, D.H., Danesh, A. and Henderson, G.D., *Visualization of oil recovery by water-alternating-gas injection using high-pressure micromodels.* SPE Journal, 2004. **9**(03): p. 290-301.
7. Gunda, N.S.K., Bera, B., Karadimitriou, N.K., Mitra, S.K. and Hassanizadeh, *Reservoir-on-a-Chip (ROC): A new paradigm in reservoir engineering.* Lab on a Chip, 2011. **11**(22): p. 3785-3792.
8. Anbari, A., Chien, H.T., Datta, S.S., Deng, W., Weitz, D.A. and Fan, J., *Microfluidic Model Porous Media: Fabrication and Applications.* Small, 2018.
9. Holtz, M., *Optimizing Permanent CO_2 Sequestration in Brine Aquifers: Example from the Upper Frio, Gulf of Mexico*. Carbon dioxide sequestration in geological media—State of the science: AAPG Studies 59, 2008, p. 1-9.